

Control of tissue morphology by Fasciclin III-mediated intercellular adhesion

Richard E. Wells^{1,2,*}, Joseph D. Barry^{3,*}, Samantha J. Warrington^{1,2}, Simon Cuhlmann⁴, Paul Evans⁵, Wolfgang Huber³, David Strutt^{1,2,‡} and Martin P. Zeidler^{1,2,‡}

SUMMARY

Morphogenesis is dependent on the orchestration of multiple developmental processes to generate mature functional organs. However, the signalling pathways that coordinate morphogenesis and the mechanisms that translate these signals into tissue shape changes are not well understood. Here, we demonstrate that changes in intercellular adhesion mediated by the transmembrane protein Fasciclin III (FasIII) represent a key mediator of morphogenesis. Using the embryonic *Drosophila* hindgut as an *in vivo* model for organogenesis, we show that the tightening of hindgut curvature that normally occurs between embryonic stage 12 and 15 to generate the characteristic shepherd's crook shape is dependent on localised JAK/STAT pathway activation. This localised pathway activity drives the expression of FasIII leading to its subcellular lateralisation at a stage before formation of septate junctions. Additionally, we show that JAK/STAT- and FasIII-dependent morphogenesis also regulates folds within the third instar wing imaginal disc. We show that FasIII forms homophilic intercellular interactions that promote intercellular adhesion *in vivo* and in cultured cells. To explore these findings, we have developed a mathematical model of the developing hindgut, based on the differential interfacial tension hypothesis (DITH) linking intercellular adhesion and localised surface tension. Our model suggests that increased intercellular adhesion provided by FasIII can be sufficient to drive the tightening of tube curvature observed. Taken together, these results identify a conserved molecular mechanism that directly links JAK/STAT pathway signalling to intercellular adhesion and that sculpts both tubular and planar epithelial shape.

KEY WORDS: *Drosophila*, Adhesion, Modelling, Organogenesis, Mouse

INTRODUCTION

Organogenesis is the culmination of multiple cellular processes. These include the regulation of cellular proliferation and tissue growth as well as the specification of the various cell fates required. Additionally, complex morphogenetic processes are also required to sculpt the resulting cells and generate the final tissue shapes and structures required for organ function.

In particular, organogenesis frequently requires the movement and rearrangement of physically associated cell populations, processes that need to be accurately choreographed over both time and space. Given the importance of these processes, the molecular mechanisms that link intercellular signalling pathways to alterations in tissue shape are comparatively poorly understood. As organogenesis in higher vertebrate models is both complex and difficult to visualise, the study of relatively simple morphogenetic processes and the use of hypothesis-based mathematical modelling to test the resulting findings has the potential to provide fundamental insights into the mechanistic underpinnings of development.

One experimentally tractable example of a three-dimensional tissue suitable for studying such morphogenetic processes is the monolayer epithelial tube of the *Drosophila* embryonic hindgut. The gut is first defined during stage 5 of embryogenesis (Hartenstein, 1993) and undergoes three asynchronous cell divisions during stage 7 (Lengyel and Iwaki, 2002). During embryogenesis, each section of the gut performs tightly regulated morphological movements and by the time the hindgut first becomes morphologically distinct at stage 10, the gut is already gently curved (Fig. 1A,B). This initial curvature is maintained through germband extension while the hindgut elongates via a convergent extension-dependent process. By stage 15, the hindgut has developed to form a shepherd's crook shape (Fig. 1D,E) characterised by a sweeping curve of $\sim 140^\circ$ and is rotated along the longitudinal axis of the embryo, breaking mediolateral symmetry (supplementary material Movie 1) (Campos-Ortega and Hartenstein, 1985). These morphogenetic processes are independent of both cell division and cell death (supplementary material Fig. S1A-H) (Iwaki et al., 2001; Lengyel and Iwaki, 2002).

One signalling mechanism central to hindgut morphogenesis is the JAK/STAT pathway (Johansen et al., 2003b; Arbouzova and Zeidler, 2006). Within the hindgut, JAK/STAT signalling is activated by the localised expression of *upd* (*os* – FlyBase) within the small intestine, a restricted expression domain that is required for correct hindgut elongation (Johansen et al., 2003b; Hombria et al., 2005). Furthermore, as pathway activation is required within the adjacent large intestine, *Upd* must act non-autonomously (Johansen et al., 2003a; Johansen et al., 2003b). Ultimately, both loss of JAK/STAT signalling or ectopic JAK/STAT activation throughout the hindgut results in truncation that is not a consequence of cell loss, but rather a failure of cell rearrangement.

Central to all morphogenetic processes are the intercellular forces that act to maintain the physical integrity of tissues. In the case of

¹MRC Centre for Developmental and Biomedical Genetics, The University of Sheffield, Firth Court, Sheffield S10 2TN, UK. ²The Department of Biomedical Science, The University of Sheffield, Firth Court, Sheffield S10 2TN, UK. ³Genome Biology, EMBL Heidelberg, Meyerhofstraße 1, 69117 Heidelberg, Germany. ⁴BHF Cardiovascular Sciences Unit, Imperial College London, Hammersmith Hospital Campus, Du Cane Road, London W12 0NN, UK. ⁵Department of Cardiovascular Science, Medical School, University of Sheffield, Beech Hill Road, Sheffield, S10 2RX, UK.

*These authors contributed equally to this work

‡Authors for correspondence (d.strutt@sheffield.ac.uk; m.zeidler@sheffield.ac.uk)

This is an Open Access article distributed under the terms of the Creative Commons Attribution License (<http://creativecommons.org/licenses/by/3.0>), which permits unrestricted use, distribution and reproduction in any medium provided that the original work is properly attributed.

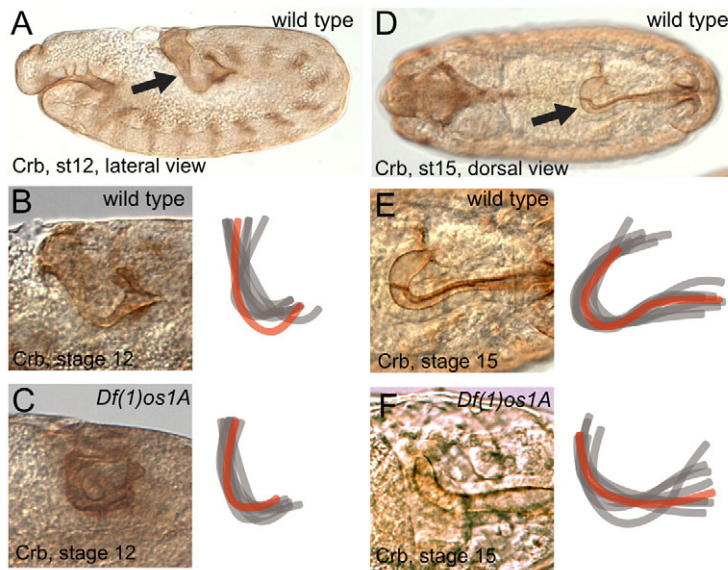


Fig. 1. Developmental changes in normal hindgut curvature. Gut lumen as visualised by Crumbs (Crb) expression. A-C are lateral and D-F dorsal views. Stages and genotypes as indicated. Hindguts pictured are shown as red overlays. (A,B) Stage 12 wild-type hindgut morphology and location (arrow in A) and an overlay of eight representative hindgut traces. (C) Hindgut shape of *Df(1)os1A* and wild-type embryos are similar. (D,E) Stage 15 wild-type hindgut morphology and location (arrow in D) and an overlay of eight representative hindgut traces. (F) Hindguts of *Df(1)os1A* embryos are less curved than wild type at this developmental stage.

the *Drosophila* hindgut, this physical integrity is dependent on intercellular junctions that exist between epithelial cells (Gumbiner, 1996; Carthew, 2005). These intercellular connections are composed of apical adherens junctions, which mediate intercellular adhesion, and more basal septate junctions (SJ), which are analogous to vertebrate tight junctions and restrict the free diffusion of solutes across epithelia.

Here, we present a novel non-septate junctional role for the normally septate junctional protein Fasciclin III (FasIII) (Snow et al., 1989) in the developing *Drosophila* hindgut – a role that is dependent on temporally and spatially localised JAK/STAT pathway signalling. Together with results derived from the analysis of wing disc folds and FasIII clonal boundaries, our findings identify a direct mechanistic link between signal transduction pathways and the biophysical processes that shape three-dimensional organs *in vivo*.

MATERIALS AND METHODS

Genetics and fly stocks

Flies were raised at 25°C on standard media. Wild-type stocks and balancers have been described by Lindsley and Zimm (Lindsley and Zimm, 1992). Other stocks used were: *Df(1)os1A*, which removes all three Upd-like JAK/STAT pathway ligands (Hombria et al., 2005), *UAS-Upd* (Zeidler et al., 1999), *UAS-DomeDcyt* (Brown et al., 2001), *UAS-hop^{ts/ml}* (Harrison et al., 1995), *10xSTATGFP* (Bach et al., 2007), *UAS-FasIII-RNAi*, *UAS-stat92E-RNAi*, *UAS-Rh4-RNAi* (Dietzl et al., 2007) and *vari^{48EP}* (Moyer and Jacobs, 2008).

The *FasIII^{A142}* mutant allele (Bellen et al., 2004) contains a *PBac*(5HPw+) insertion within the first intron of *FasIII* and produces no detectable protein (Fig. 5A). Mutants are homozygous viable but male sterile, with offspring both homozygous for the *A142* insertion and trans-heterozygous with other alleles giving homozygous progeny at Mendelian ratios with similar hindgut curvature phenotypes (supplementary material Fig. S2). Clones lacking STAT92E were generated in *Ubx-FLP; FRT82B stat92E^{56D3} / FRT82B Ubi-GFP* larvae whereas clones lacking FasIII were generated in *Ubx-FLP; FasIII^{A142} FRT40A / Ubi-GFP FRT40A* larvae. Gal4-expressing lines used were: *10xSTATGFP*, *ptc-Gal4*, *UAS-DsRed* (Vidal et al., 2010), *Zfh2-Gal4* (Capdevila and Guerrero, 1994), *byn-Gal4* and *byn-Gal4, UAS-GFP* (Iwaki et al., 2001).

Molecular biology

UAS-FasIII was generated from cDNA clone RE66907 (Stapleton et al., 2002), which represents the 401 amino acid RB splice form. This was

cloned into pUAST (Brand and Perrimon, 1993) and pAc5.1 (Invitrogen) for transformation and expression in cultured cells, respectively.

For immunoprecipitation, lysates were prepared from a mixed embryo collection aged from stage 13 to 15 and incubated with anti-Vari (1:50; Moyer and Jacobs, 2008) and anti-FasIII [1:100; Developmental Studies Hybridoma Bank (DSHB)] overnight. Protein complexes were isolated using Protein-G coupled Dynabeads (Invitrogen). Western blots were undertaken using standard SDS/PAGE technique and probed with anti-FasIII (1:100).

Tissue culture

Kc₁₆₇ cells were grown in Schneider's medium supplemented with 5% foetal calf serum (Schneider, 1972). Cells were transfected with *pAct-FasIII* using Effectene (Qiagen) and allowed to express for four days before fixation.

Immunohistochemistry and live imaging

Tissue collection, fixation and antibody staining was undertaken as described (Zeidler et al., 1999; Wright et al., 2011). The following primary antibodies and concentrations were used: mouse anti-FasIII (1:100; DSHB), anti-E-cad (1:25; DSHB), mouse anti-Crb (1:10; DSHB), mouse anti-Dlg (1:50; DSHB), mouse anti-FasII (1:20; DSHB), mouse anti-Cor (1:20; DSHB), rabbit anti-Vari (1:50) (Moyer and Jacobs, 2008), anti-cleaved Caspase 3 (1:100; Abcam), rabbit anti-Histone H3-phosphoS10 (1:100; Abcam).

Microscopy was undertaken using a Zeiss LSM 510 META, Leica SP1 and a Zeiss Axioskop 2 MOT. Single confocal slices were taken for both hindgut and wing disc images. Confocal images of cells are maximum projections of stacks.

In situ hybridisation was undertaken as described by Lehmann and Tautz (Lehmann and Tautz, 1994). *FasIII* digoxigenin-labelled RNA probes were generated from PCR products amplified from cDNA clone RE66907 (Stapleton et al., 2002) using AGGTCATGTCCTCGACCAAC and GAATTAATACGACTCACTATAGGGAGAAAAACACCATCGGCCAG-TAG primers. The *Socs36E* probe was generated from the EST SD04308.

For live imaging, embryos were hand dechorionated and mounted on a heptane glue coverslip rotated dorsally then covered with halocarbon 700 (Halocarbon Products Corporation). Images were obtained using a PerkinElmer UltraVIEWVoX spinning-disk confocal microscope at intervals of two minutes. Image processing was undertaken using Volocity (PerkinElmer).

Hindgut angle measurements

Embryonic hindguts were visualised using Crb staining and photographed using a Zeiss Axioskop 2 MOT microscope. The anterior and posterior extremes of dorsally oriented embryos were used to define the midline and

a line linking the distal hindgut-midgut boundary to the anterior of the hindgut curve where it meets the midline were marked. The angle at which the lines meet was then measured using ImageJ. Average angles were measured for each genotype and Student's *t*-tests used to establish statistical significance.

FasIII at clonal boundary quantification

Images representing single confocal sections of the wing imaginal discs stained with anti-FasIII and which include FasIII clonal boundaries were used. Regions of interest encompassing *+/+* and *+/-* boundaries were analysed to provide the mean fluorescence intensity, and cell centre background was subtracted from each boundary value. Given the FasIII contribution from two adjacent wild-type cells, values from *+/+* were halved. Average fluorescence intensities of 33 cells measured from five independent images were compared using a two-tailed paired *t*-test.

10xSTATGFP intensity measurements

Asymmetry of 10xSTATGFP reporter activity was established by quantifying reporter GFP levels and comparing this with GFP expressed ubiquitously via *byn > GFP*. ImageJ was used to measure the intensity of GFP at equal distances from the small intestine-large intestine boundary on both the inside and the outside of the hindgut curve. Results are represented by the inner:outer ratio of GFP. Significance was calculated using Student's *t*-test.

Mathematical quantification of boundary curvature

The curvature of clonal boundaries was measured from single confocal images of seven *FasIII* mutant and six control imaginal discs captured using a 20× multi-immersion objective. Images were converted to greyscale, contrast optimised and anonymised before boundaries separating mutant (GFP^{-/-}) from heterozygous (GFP^{-/+}) and wild type (GFP^{+/+}) were manually drawn at the computer. Resulting boundaries were then parsed by a pixel-linking algorithm to generate individual clonal boundaries before the localised curvature of each individual boundary was measured using smoothing windows of 5, 10 and 15 μm. Small segments <15 μm length were rejected from further analysis and results for each genotype binned to give *n*=164 (controls) and *n*=113 (*FasIII* mutants) individual segments, which were compared using two tailed Mann-Whitney tests. FasIII clonal boundaries were significantly straighter (*P*<0.002) at all three resolutions. Data from the 15 μm resolution is shown in Fig. 5E. A detailed description of the line curvature analysis approach used and the 2D hindgut model generated is presented in the supplementary material Appendix S1.

En face immunostaining of PECAM-1

The expression levels of PECAM-1 (also known as CD31) in endothelial cells were assessed at the inner and outer curvatures of the murine aortic arch by en face staining (Hajra et al., 2000; Zakkar et al., 2008). The experiment was conducted following guidelines set out by the Federation of European Laboratory Animal Science Associations. Six male C57BL/6 mice between 2 and 3 months of age were studied. Animals were killed by CO₂ inhalation. Aortae were perfused *in situ* with PBS and then perfusion-fixed with 2% formalin prior to harvesting. Fixed aortae were immunostained using FITC-conjugated anti-CD31 antibodies (Biosciences Pharmingen). Nuclei were identified using TO-PRO-3 (Invitrogen). Stained vessels were mounted prior to visualisation of endothelial surfaces *en face* using confocal laser-scanning microscopy (Zeiss LSM 510 META). PECAM-1 expression was quantified for multiple cells (>100 per site) using LSM 510 software (Zeiss) and calculation of mean fluorescence intensities (MFI) with standard error of the mean. Differences between samples were analysed using an unpaired Student's *t*-test.

RESULTS

JAK/STAT signalling is required for normal hindgut curvature

Given the previously described role of the JAK/STAT pathway in *Drosophila* hindgut elongation (Johansen et al., 2003b), we set out to determine whether pathway signalling played any other roles in the development of this structure. By comparison to the hindguts of

wild-type individuals (Fig. 1A,B), the hindguts of embryos hemizygous for *Df(1)os^{1A}*, which lack the genes encoding all three JAK/STAT-pathway ligands (Hombria et al., 2005), are normal at stage 12 (Fig. 1C). This suggests that the initial stages of hindgut specification do not require JAK/STAT pathway signalling. However, by stage 15 defects in the overall shape and curvature of hindguts lacking JAK/STAT pathway activity are clearly visible with a qualitative reduction in the tightness and shape of the curve being apparent (compare Fig. 1E and 1F; see Fig. 2G).

In the light of the reduced curvature in JAK/STAT pathway mutants, we set out to identify the reason for this phenotype. A similar failure-to-tighten phenotype is also apparent in individuals uniformly expressing a dominant-negative pathway receptor throughout the developing hindgut via *byn-Gal4/UAS-DomeAcyt* (compare Fig. 2A and 2B), demonstrating that the requirement for the JAK/STAT pathway is intrinsic to the hindgut itself. Furthermore, ectopic activation of the JAK/STAT pathway in the hindgut via the misexpression of either the Unpaired (Upd) ligand (Fig. 2C) or the cell autonomously acting activated JAK allele *hop^{timl}* (Luo et al., 1995) (Fig. 2D) are also sufficient to induce a qualitatively similar failure in hindgut curvature.

Quantification of hindgut curvature confirms that the reduction in curvature apparent at stage 15 following both the loss and ectopic activation of JAK/STAT signalling is statistically significant (Fig. 2G) and indicates that normal JAK/STAT pathway activity is required to tighten the initial curve present in the stage 12 hindgut. Taken together, these results identify a novel developmental role for pathway signalling and suggest that spatially regulated wild-type levels of JAK/STAT activity are autonomously required within the gut to promote normal curvature.

Asymmetric JAK/STAT signalling acts via FasIII in the hindgut

To understand better the cause of the failure-to-tighten hindgut phenotype, we first examined spatial aspects of JAK/STAT pathway activity in the hindgut using an *in vivo* STAT92E activity reporter (Bach et al., 2007). In order to provide spatial reference, we visualised Crumbs (Crb) as a marker for apical epithelial membranes, and the boundary between the anterior small intestine in which Upd is expressed (Fig. 3A, hatched area) and the adjacent large intestine. Strikingly, 10xSTATGFP reporter activity, and hence pathway activation, is highly asymmetric within the anterior of the stage 14 large intestine. Cells on the inside of the hindgut curve show higher pathway activity than cells at comparable distances from the Upd-expressing large intestine on the outside of the curve (Fig. 3A, white arrows). This difference in reporter activity is significant and not a consequence of increased cell density as expression of GFP throughout the hindgut results in approximately uniform levels of GFP (Fig. 3B). Furthermore, asymmetry in reporter activity is mirrored by expression of the endogenous JAK/STAT pathway target gene *Socs36E* (supplementary material Fig. S3A-C) (Karsten et al., 2002).

One candidate effector gene that is potentially downstream of pathway signalling in the hindgut is Fasciclin III (FasIII; Fas3). In addition to containing multiple potential 3n and 4n STAT92E binding sites within the genomic locus (supplementary material Fig. S4A) (Rivas et al., 2008), FasIII protein is almost completely lacking in *upd* mutant embryos (supplementary material Fig. S4B-F). Furthermore, *FasIII* mRNA is expressed in the developing hindgut in a pattern that not only overlaps *Socs36E* mRNA expression, but is also strongly reduced by expression of the dominant-negative pathway receptor *DomeAcyt* (supplementary

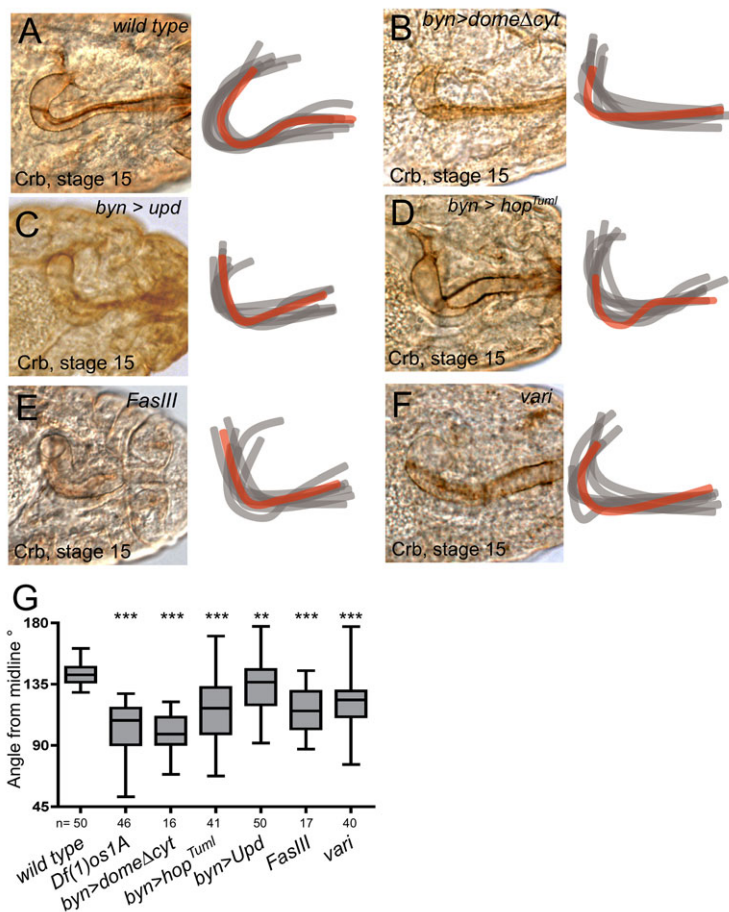


Fig. 2. Disruption of hindgut curvature downstream of JAK/STAT signalling. Dorsal views of stage 15 gut lumens as visualised by Crumbs (Crb) expression. Hindguts pictured are shown as red overlays. (A-F) Representative images of the indicated genotypes with overlays of eight hindgut traces. (G) Box plot of stage 15 hindgut angles in the indicated genetic backgrounds. Number of samples measured for each genotype are shown. Box represents 25th to 75th percentile; line represents the median; whiskers represent min/max values. *** $P < 0.0001$, ** $P < 0.001$.

material Fig. S3D-I) (Brown et al., 2001). Consistent with its identification as a putative target gene, FasIII protein levels are detected within the developing hindgut curve in a pattern that mirrors the asymmetry of JAK/STAT activity at comparable stages (Fig. 3C-F). During embryonic stages 12-13, FasIII is detected exclusively in cells on the inside of the hindgut (Fig. 3C,D), whereas starting from stage 14, expression along the inside of the curve is supplemented by increasing levels of FasIII expression in cells that make up the outside of the curve (Fig. 3E,F, arrows). In addition to changes in protein level, the subcellular distribution of FasIII also alters during development. Strikingly, and in contrast to the previously described role of FasIII as a septate junction protein, cells making up the inside of the curve contain FasIII distributed along the entire length of the lateral cellular membranes (Fig. 3C-E, arrowheads). This lateralisation corresponds with the increased levels of *10xSTATGFP* reporter activity detectable at this stage (Fig. 3G) and occurs during the developmental window in which the hindgut curve is tightened in wild-type embryos (Fig. 1A,D). We therefore examined what role FasIII might play in this process. In embryos homozygous for the strong loss-of-function *FasIII^{Δ142}* allele (which expresses no detectable protein; see Materials and methods), mutant embryos show a reduction in stage 15 hindgut curvature, similar to those lacking JAK/STAT signalling (Fig. 2E,G), a phenotype that is mirrored in trans-heterozygous allelic combinations (supplementary material Fig. S2). This suggests that the failure of mutants lacking JAK/STAT signalling to tighten curvature is likely to be mediated primarily through the pathway target gene *FasIII*. Consistent with this model, embryos

hemizygous for *Df(1)os^{LA}* (Hombria et al., 2005), which lack all JAK/STAT pathway ligands, no longer express FasIII asymmetrically and lateralised distribution is no longer detectable along the inside of the hindgut curve. Rather, only junctional FasIII appearing at stage 15 (Fig. 4D) is detected, suggesting that subsequent FasIII expression is controlled by a JAK/STAT-independent process.

Having established the link between FasIII lateralisation and JAK/STAT pathway activity, we set out to examine the situation following ectopic pathway activation. As expected, uniform JAK/STAT pathway activation mediated by the ubiquitous expression of *Hop^{TumI}*, as well as overexpression of *FasIII* mRNA, uniformly increases FasIII protein levels, an increase that overlays the endogenous asymmetry of expression (Fig. 4E-F'). Notably, this overexpression is sufficient to cause the lateralisation of FasIII protein around the outside of the curve (Fig. 4E-F', arrowheads), suggesting that FasIII lateralisation can be induced simply by increasing FasIII protein levels.

By contrast to the pattern of JAK/STAT-dependent expression at earlier stages, beginning at stage 14/15 FasIII starts to be expressed throughout the hindgut in a JAK/STAT pathway-independent manner (Fig. 4D). FasIII also becomes restricted to sub-apical regions of lateral membranes (Fig. 3E,F, arrows), a localisation that overlaps with that of other septate junction proteins including Varicose (Vari) (Fig. 3G'''), Discs Large (Dlg; Dlg1), Fasciclin II (FasII; Fas2) and Coracle (Cora) (Fig. 4A-C). The restriction of FasIII to sub-apical domains on both the outside and inside of the hindgut from stage 14 is consistent with the

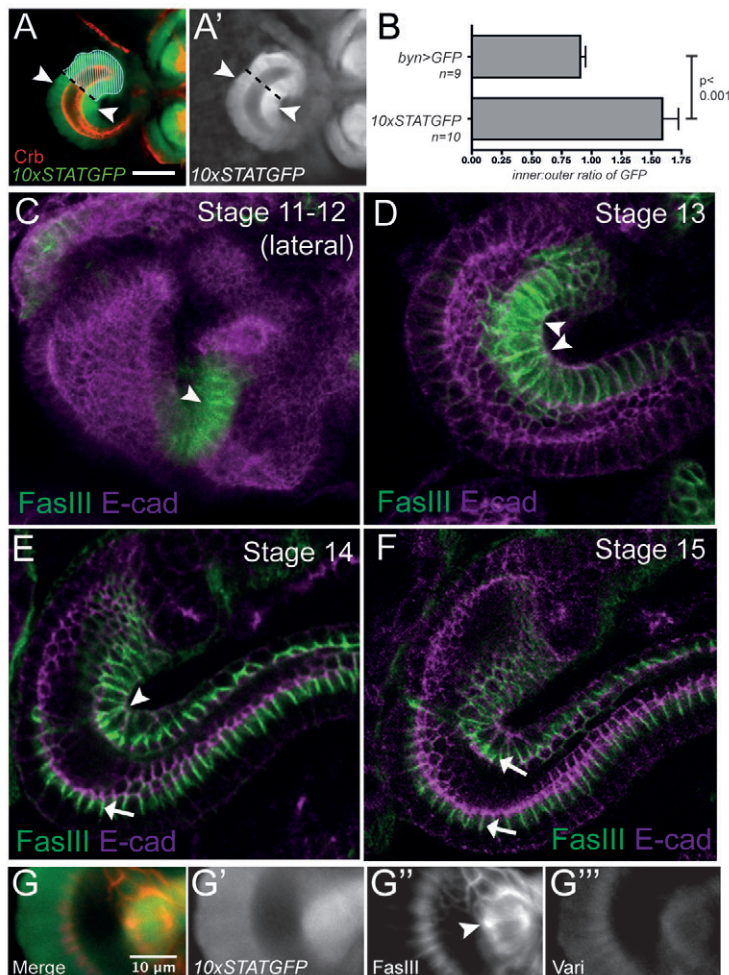


Fig. 3. Asymmetry of JAK/STAT signalling and FasIII. Dorsal views of hindguts of the indicated stages. (A) *10xSTATGFP* reporter and Crumbs (Crb) expression. Upd expression domain is marked by hashes. Reporter intensity was measured in cells (arrowheads) equidistant from the small intestine-large intestine boundary (dashed black line). Scale bar: 30 μ m.

(B) Quantification of *10xSTATGFP* levels on opposite sides of the hindgut compared with the same points in controls expressing GFP uniformly (*byn >GFP*). Fluorescence is shown as a ratio of inner:outer intensity. Error bars represent s.e.m. (C-F) Time course of FasIII expression (green) within the developing hindgut counterstained with the adherens junction marker E-cad (magenta). View is lateral at stage 11-12 (C) and dorsal in subsequent stages. FasIII expression is restricted to the inside of the hindgut curve in C,D and is located along the entire lateral margin of the cells (arrowheads). Septate junctional FasIII (basal to E-cad) is detected from stage 14 (E,F, arrows). (G-G'') Lateralised FasIII (G'', red in merge) on the inside of the hindgut curve overlying the region of higher *10xSTAT-GFP* reporter activity (G', green in merge) and Varicose (G''', blue in merge) expression.

behaviour of components of the developing septate junction (Tepass and Hartenstein, 1994). Furthermore, this also suggests that lateralised FasIII on the inside of the curve, and not present within sub-apical domains, is likely to play a non-septate junctional role during stage 12 to 15 of embryonic development.

Taken together, these data suggest that during normal development increased levels of JAK/STAT pathway activity on the inside of the hindgut stimulate increased FasIII expression that, in turn, leads to FasIII lateralisation.

We next examined FasIII lateralisation in embryos lacking the MAGUK scaffold protein Varicose (Vari), a factor required for septate junction formation and the recruitment of FasIII to septate junctions during stage 14 (Moyer and Jacobs, 2008). Although loss of Vari does not change FasIII protein levels, it does result in ectopic lateralisation of the low levels of endogenous FasIII expressed around the outside of the curve during stage 14 (Fig. 4G,G', arrowheads). Strikingly, hindgut curvature in stage 15 *vari* mutants is reduced to an extent similar to that resulting from the complete loss of FasIII (Fig. 2F,G). This phenotype is independent of differences in FasIII protein expression levels on opposing sides of the gut and is likely to occur after the initial FasIII lateralisation. Although it is possible that other factors might also be disrupted by the lack of Vari, this result is consistent with a hypothesis in which lateralisation of FasIII represents the key factor required for normal hindgut curvature. Consistent with a requirement for Vari in septate junction formation and FasIII

localisation, co-immunoprecipitation assays from wild-type embryos also suggest that Vari physically interacts with FasIII (Fig. 4H).

Finally, it should be noted that the hindgut curvature phenotype associated with *vari* mutants occurs in embryos that have hindguts of normal length (Fig. 2F), suggesting that the curvature phenotypes associated with loss of JAK/STAT activity are not a consequence of a failure in convergent extension and hindgut elongation.

FasIII, adhesion and tissue shape

Molecularly, FasIII is a transmembrane protein with extracellular immunoglobulin (Ig) domains and has previously been suggested to act as a homophilic adhesion molecule (Snow et al., 1989). In order to test this prediction in an *in vivo* context, we generated clones of cells homozygous for the *FasIII^{A142}* allele in the developing wing imaginal disc. We found that wild-type cells adjacent to *FasIII* mutant cells preferentially localise endogenous FasIII to those junctions shared with other wild-type cells (Fig. 5A,A', arrowheads). When quantified, 33 independent cells contained an average of 66.8 fluorescence units at homotypic boundaries versus 1.4 at heterotypic interfaces (following background subtraction). Correcting for FasIII contributed by two cells at homotypic boundaries, this represents a 24-fold enrichment ($P < 0.0001$). These results indicate that FasIII preferentially forms homophilic intercellular connections *in vivo*. Consistent with our findings in imaginal disc epithelia, we also find that expression of FasIII in

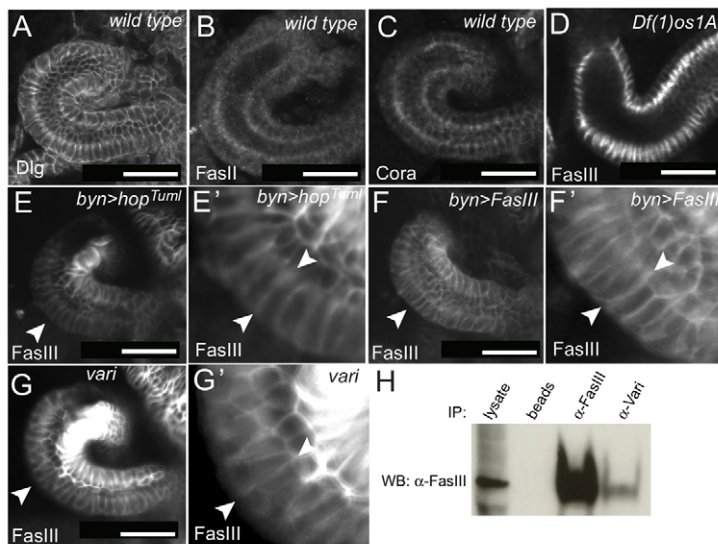


Fig. 4. FasIII subcellular localisation. Dorsal views of stage 13/14 hindguts of the indicated genotypes and stained with the indicated antibodies. (A-C) Septate junction proteins Discs Large (Dlg), Fasciclin II (FasII) and Coracle (Cora) are symmetrically distributed and localised in sub-apical regions. (D-E') Overview and magnification of FasIII localisation in stage 13 hindguts in JAK/STAT loss- and gain-of-function backgrounds. Arrowheads indicate examples of lateralised FasIII. (F-F') FasIII is lateralised around the outside of a stage 13 hindgut (arrowheads) following its overexpression. (G,G') Asymmetrical FasIII expression and ectopic lateralisation on the outside of the curve (arrowheads) in *varicose (vari)* mutants. (H) Co-immunoprecipitation from wild-type embryos using the indicated antibodies and blotted (WB) with anti-FasIII indicates a co-precipitation of FasIII with Vari. Scale bars: 30 μ m.

normally semi-adherent Kc_{167} cells drives formation of clumps comprising only FasIII-expressing cells (Fig. 5B). Furthermore, these clumps localise FasIII along their flattened common surface (Fig. 5B, arrowheads), a morphology that confirms the homophilic nature of FasIII association and indicates that FasIII mediates intercellular adhesion sufficient to flatten the plasma membrane at these intercellular contacts. This adhesion is apparent even in the absence of septate or adherens junctions (which are not present in this haematologically derived non-epithelial cell line) and suggests that the lateralised FasIII present in the hindgut is sufficient to increase adhesion locally between these cells.

Finally, we also examined the overall morphology of clonally related groups of wild-type and *FasIII* mutant cells generated in wing imaginal discs (Fig. 5C-E). Control imaginal discs containing GFP-marked, but otherwise wild-type, clones have jagged clonal boundaries (Fig. 5C), a pattern that represents the consequence of normal cell mixing that occurs during the development of the wing disc between clonal induction and late third instar. By contrast, clones removing FasIII have boundaries that appear qualitatively straighter (Fig. 5D); this rounded clone phenotype has previously been described as being indicative of changes in intercellular adhesion (Wei et al., 2005), an effect also supported by *in silico* modelling (Graner and Glazier, 1992). In order to confirm this qualitative difference, we quantified the curvature of clonal boundaries under both conditions. The boundaries between GFP- and GFP+ tissue in wing discs containing FasIII clones and wild-type controls were manually segmented and then mathematically quantified for local line curvature (supplementary material Appendix S1). This confirmed that boundaries between FasIII expressing and non-expressing cells show an approximate 25% reduction in local curvature ($P < 0.0001$) (Fig. 5E). This is consistent with physiological levels of FasIII expression altering intercellular adhesion between epithelial cells in the wing imaginal disc.

A mathematical model for FasIII-dependent hindgut curvature

We hypothesised that the curvature phenotypes associated with loss of *FasIII* may be a direct consequence of the adhesive activity of FasIII, which directly regulates the physical forces between neighbouring hindgut cells. For homotypic adhesive contacts mediated by cadherins, it has been suggested that a primary

mechanism driving increased cell-cell contact area is a decrease in local surface tension (Lecuit and Lenne, 2007; Manning et al., 2010). In this scenario, increased intercellular adhesion reduces the net force per length (or equivalently, energy per area), which acts normal to the plasma membrane and opposite to the outward acting cell pressures. This differential interfacial tension hypothesis (DITH) (Brodland, 2002) suggests that a decrease in local surface tension leads to an increase in adhesive contact area in order for the tissue to attain a lower energy conformation. From the perspective of global tissue morphology, this also results in changes to the aspect ratio of the cell in order for the cells to maintain a fixed volume.

Guided by the idea that FasIII lateralisation is likely to increase the area over which adjacent cells form FasIII:FasIII intercellular connections, we speculated, based on the DITH, that FasIII may be directly reducing local surface tension across the entire lateral membrane. As feasible methods for measuring surface tension *in vivo* are lacking, we constructed a mathematical model based on the DITH in order to predict how local changes might affect global tissue shape and hindgut curvature phenotypes, as well as to determine the magnitude of the hypothesised FasIII-mediated surface tension change that would be required.

The model (supplementary material Appendix S1) is based on the principle of tissue surface energy minimisation and makes simplified assumptions about local geometric constraints, notably a constant gut diameter and fixed connection to the rectum (R in Fig. 6). Using *in vivo* data to define the number of cells present along the length of the hindgut, a straight tubular 'starting point' model was generated (Fig. 6A) and simulations were run in which the surface tension parameter $\hat{\sigma}$ was set uniformly for all lateral membranes prior to 1000 rounds of energy minimisation (Fig. 6E). For a particular set of parameter values where $\hat{\sigma} = 0.5$, the model generated a morphology with an angle of 111° (Fig. 6B), approximating that found in *Df(1)os^{1A}* and *FasIII* mutants (Fig. 2G). In order to represent the intercellular adhesion mediated by lateralised FasIII, we then progressively reduced $\hat{\sigma}^{FasIII}$ (supplementary material Appendix S1) along the lateral membranes of the 18 cells making up the inside of the hindgut curve (Fig. 6C, red membranes) before determining a new lowest energy state (Fig. 6E). Strikingly, localised reductions in surface tension between just these 18 cells were sufficient to tighten the overall angle of the curve across a range of values (Fig. 6C,F; supplementary material

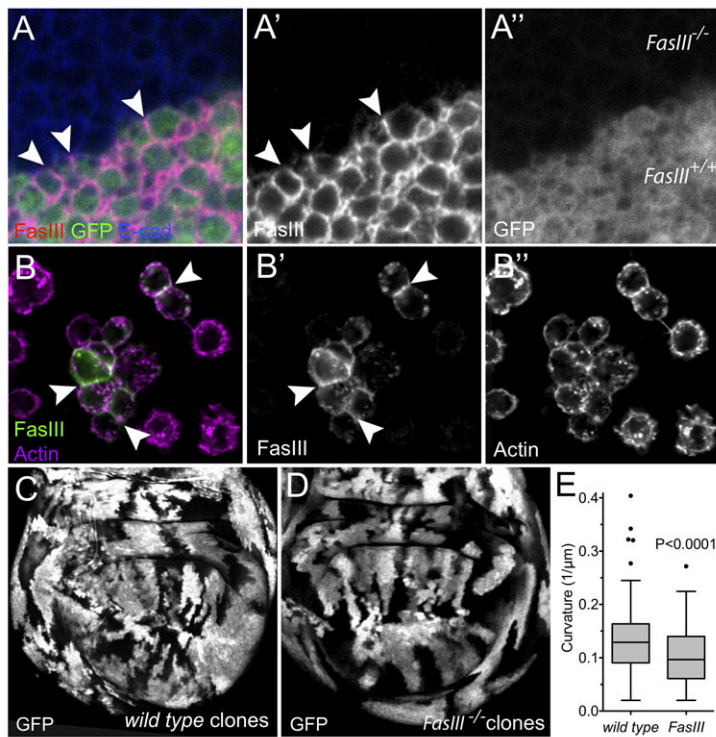


Fig. 5. FasIII is a homophilic adhesion molecule. (A–A'') Clonal boundary within a third instar wing imaginal disc containing regions lacking FasIII (*FasIII*^{-/-}) and wild-type regions (*FasIII*^{+/+}). FasIII is preferentially localised on intercellular boundaries shared by wild-type cells (arrowheads). (B–B'') Exogenously expressed FasIII and endogenous F-Actin in Kc₁₆₇ tissue culture cells. FasIII is localised on plasma membranes abutting other FasIII-expressing cells (arrowheads). Note that 100% of FasIII expressing cells are seen in clumps, and non-expressing cells are never seen in clumps. (C,D) Third instar wing imaginal discs containing GFP labelled, but otherwise wild-type (C) or *FasIII*^{A142} mutant (D) clones. (E) Quantification of average clonal boundary curvature using a 15- μm smoothing window (as described in Materials and methods). Box represents 25th to 75th percentile; line represents the median; whiskers were calculated using the Tukey method with outliers shown. *P*-value was determined by a two-tailed Mann–Whitney test.

Movie 2), and hence modified global tissue shape. A reduction to $\hat{\sigma}^{\text{FasIII}} = 0.35$ was sufficient to generate a hindgut angle approximately equivalent to that measured in wild-type embryos (136° ; Fig. 2G). This value of $\hat{\sigma}^{\text{FasIII}}$ corresponded to a reduction in local surface tension of 30%, a physiologically plausible change sufficient to account for the normal tightening of the hindgut curve observed *in vivo*.

One puzzling aspect of the primary *in vivo* data is the reduction in hindgut curvature following both the removal and the over-activation of JAK/STAT signalling (Fig. 2). To test whether the DITH model could additionally provide a mechanistic explanation for these counter-intuitive phenotypes, we proceeded to simulate the effect of uniformly lateralising FasIII throughout the hindgut, a consequence of uniformly activating JAK/STAT signalling (Fig. 4E,E'). Starting from a ground state corresponding to a lack of FasIII where $\hat{\sigma} = 0.5$ (Fig. 6B), we simulated ubiquitous FasIII lateralisation by uniformly reducing $\hat{\sigma}$ to 0.35 before determining the new minimal energy state. Strikingly, this global change in surface tension resulted in only minor changes in angle (114° ; Fig. 6D). This result supports the view that it is the localised asymmetry of FasIII lateralisation that represents the key factor in tightening the hindgut curve while simultaneously demonstrating a mechanism to explain the similar phenotypes exhibited in both JAK/STAT loss- and gain-of-function mutations *in vivo*.

An additional prediction of the DITH model is the lengthening of lateral membranes along the inside of the hindgut curve (Fig. 6C, compare l_i and l_o ; supplementary material Fig. S5F). As we had not previously noticed such an effect *in vivo*, we retrospectively examined both wild-type and *Df(1)os^{1A}* embryos and measured the ratio of lateral membrane lengths on opposite sides of the curve (Fig. 6G). As predicted by the DITH model, lateral membranes of cells along the inside of the wild-type curve are indeed longer than those opposite in which FasIII is not lateralised; this validates the model that supports the DITH approach and is consistent with the

increased intercellular adhesion likely to be elicited by FasIII in these cells. A competing DITH model that treated the connection to the midgut as fixed was also tested but failed to simultaneously give accurate predictions for gut angle and the extent of membrane lengthening across a range of simulation parameters (supplementary material Appendix S1), indicating that each readout is not a trivial consequence of the other.

JAK/STAT signalling, FasIII and tissue folds in the wing disc

Given the requirement for FasIII in hindgut curvature described above, we investigated whether FasIII might represent a more widely conserved mechanism for tissue shape remodelling. The late third instar wing imaginal disc consists of a columnar epithelial sheet that contains three distinct folds within the presumptive dorsal hinge region. We term these the proximal, medial and distal folds (labelled P, M and D in Fig. 7). As demonstrated by the *10xSTATGFP* pathway activity reporter, cells within the trough of the medial and proximal folds have high levels of JAK/STAT signalling (Fig. 7A,B, green). Furthermore, FasIII in these cells is partially lateralised (Fig. 7B', arrowhead). By contrast, the distal fold has low JAK/STAT activity and FasIII is principally sub-apical (Fig. 7B,B'). To examine a potential link between JAK/STAT signalling, FasIII and fold integrity, we expressed *in vivo* RNAi constructs within the *patched* (*ptc*) expression domain (Fig. 7A, red). As expected, knockdown of *Stat92E* mRNA reduces *10xSTATGFP* reporter activity (loss of green in Fig. 7C). An *xz* section through a control region shows wild-type fold morphology (Fig. 7D), whereas sections through the *ptc* domain show a marked shallowing and apical opening of the P and M folds (Fig. 7E,F). Given that this phenotype is observed in the regions in which the JAK/STAT pathway is normally active, this suggests that pathway signalling is involved in the establishment of wing disc folds. Using a similar approach,

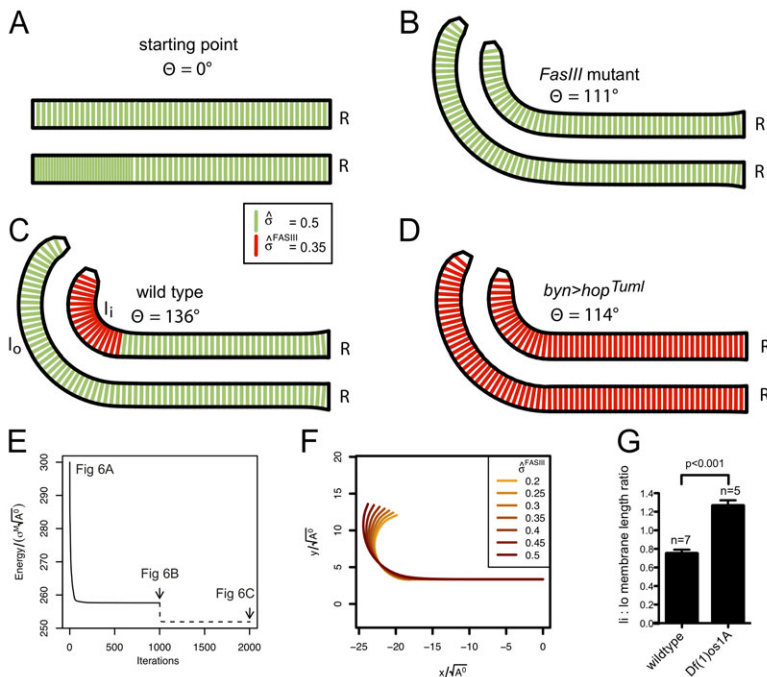


Fig. 6. Modelling FasIII-induced adhesion in the hindgut.

Two-dimensional representations of the stage 15 *Drosophila* hindgut showing lateral membranes (green). Vertices in contact with the rectum (R) are fixed during all of the simulations. (A) Initial topology of hindgut structure. (B) Surface energy minimised hindgut model for $\delta = 0.5$ representing the *FasIII* mutant condition. The angle with respect to the midline is 111° . (C) The effect of lateralised FasIII (red membranes) in 18 red lateral membranes where $\delta^{FasIII} = 0.35$. The angle with respect to the midline increases to 136° ; also note the increase in the length of the lateral membranes of cells on the inside of the curve (l_i) relative to the outside of the curve (l_o). (D) Simulation of uniformly lateralised FasIII ($\delta^{FasIII} = 0.35$). Angle with respect to the midline is now 114° . (E) Energy functions of the hindgut structures shown in A-C after 1000 successive iterations of the conjugate gradient method. The energy axis is dimensionless as energy is scaled by $\sigma^M \sqrt{A^0}$. (F) Tracks showing the change in the morphology of the hindgut over the range $0.2 \leq \delta^{FasIII} \leq 0.5$. (G) Ratio of lateral membrane length on the inside:outside ($l_i:l_o$) of wild-type and *Df(1)os1A* embryos. Error bars represent s.e.m.

RNAi targeting of *FasIII* mRNA in the *ptc* domain strongly reduces FasIII protein levels (loss of red in Fig. 7G). Furthermore, by comparison to control regions in which FasIII is present (Fig. 7H), loss of FasIII also leads to an opening of the apical region of the M fold and a reduction in its overall depth (compare arrowheads in Fig. 7I,H). In order to validate this finding, we also used *Zfh2-Gal4*, which is expressed throughout the M fold region (Fig. 7J, red). As expected, RNAi expression targeting both *Stat92E* and *FasIII* mRNA specifically driven by *Zfh2-Gal4* was also sufficient to disrupt the M fold (Fig. 7K-M). Interestingly, imaginal discs from homozygous *FasIII* mutants (in which FasIII is uniformly removed from the tissue) appear to have normal fold morphology, consistent with the effects of loss of FasIII being strongest when sharp boundaries of expression are present.

These results show that localised loss of JAK/STAT pathway signalling and FasIII are both sufficient to cause a disruption in the development and/or maintenance of fold integrity within the wing imaginal disc. Taken together, they also suggest that the FasIII-modulated regulation of intercellular adhesion might represent a general mechanism by which organs are shaped during development.

DISCUSSION

Here we describe how altered intercellular adhesion mediated by FasIII plays a key role in the development of tissue shape and in particular curvature in epithelially derived organs. We demonstrate that FasIII is a homophilic adhesion molecule and have developed a mathematical model that replicates *in silico* the changes mediated by FasIII *in vivo*. Together, our findings support the view that the phenotypes seen upon loss or gain of FasIII activity can be explained by changes in intercellular adhesion.

FasIII in the hindgut

We have shown that JAK/STAT pathway activation in the stage 12-14 hindgut is asymmetric and that this causes an increase in FasIII protein expression in cells along the inside of the hindgut curve. This increase is sufficient to cause FasIII lateralisation beyond septate junctions, a sub-cellular redistribution that we propose is

necessary for normal hindgut curvature. The mechanistic basis underlying the initial asymmetry in JAK/STAT pathway activation is unclear; however, one potential cause is an underlying asymmetry in the interaction of Upd with the extracellular heparin sulphate proteoglycans Dally and/or Dally-like (Hayashi et al., 2012). Although we do not observe any asymmetry in Dally-like expression (not shown), differences in the distribution of Dally or the post-translational modification of either heparan sulfate proteoglycan (HSPG) might be present.

No matter what the mechanistic basis, pathway asymmetry in the stage 12-14 hindgut results in high levels of FasIII expression around the inside of the hindgut curve. Under these conditions, the resulting lateralisation of FasIII leads to an increase in the contact area over which juxtaposed FasIII in adjacent cells can interact. Consistent with our results from cell culture assays, this increase in FasIII:FasIII contact area is thought to cause an increase in intercellular adhesion. The DITH model suggests that this is sufficient to increase total lateral membrane area, and hence further increase FasIII:FasIII contact area. We envisage that once FasIII has escaped from its normal sub-apical junctional position, this process may be self-reinforcing in nature, offering an adhesive zipper mechanism by which tissues locally remodel their geometry in response to external signalling cues.

FasIII-mediated adhesion and junctions

One intriguing finding is that the intercellular adhesive effect mediated by both the loss and overexpression of FasIII is independent of both adherens junctions and other septate junction protein components. In the case of septate junctions, tissue culture cell aggregation assays suggest that FasIII homotypic adhesion is effective even in the absence of other septate junction proteins (which are not present in *Kc167* cells). Furthermore, lateralisation-induced hindgut curvature occurs at developmental stages when septate junctions have not yet formed (Oshima and Fehon, 2011).

In addition, changes in intercellular adhesion are also evident along the boundary of FasIII loss-of-function clones in the wing disc, where they are sufficient to lead to a significant straightening

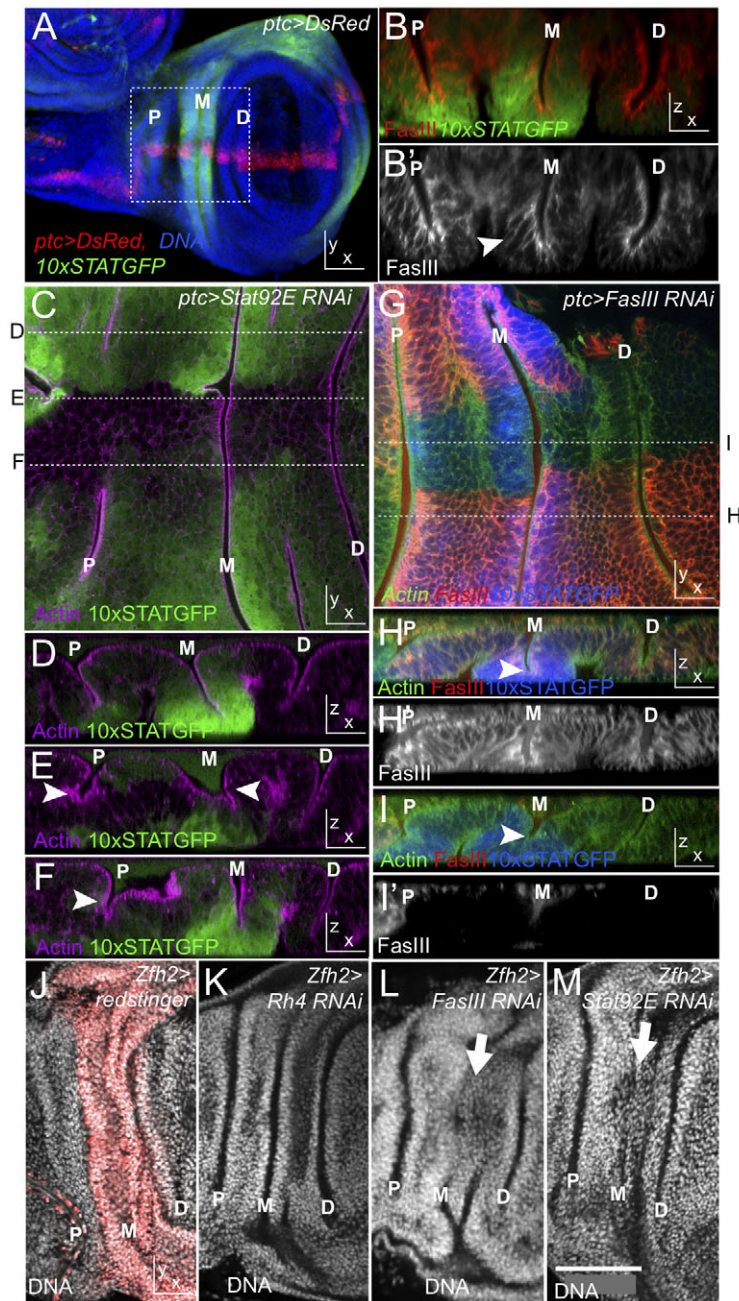


Fig. 7. JAK/STAT signalling and FasIII in wing disc hinge folds.

Third instar wing imaginal discs are shown with ventral to the right. The position of the proximal (P), medial (M) and distal (D) folds are indicated. Genotypes as indicated. **(A)** Wild-type disc showing *10xSTATGFP* reporter activity, the *ptc-Gal4* expression domain and DNA. The dotted box indicates the region shown in C, G, J-M. **(B, B')** xz section through the midline of a third instar wing disc showing *10xSTATGFP* reporter and FasIII expression. Arrowhead indicates lateralised FasIII. **(C)** xy image of a *10xSTATGFP* containing wing disc expressing an RNAi targeting *Stat92E* mRNA. Loss of reporter activity indicates RNAi efficacy and expression domain. Dotted lines indicate the positions of the indicated xz sections shown in D-F. **(D-F)** xz sections of the disc shown in C showing fold morphology. Disruptions of the M and P folds are indicated by white arrowheads. **(G)** xy image of a *10xSTATGFP*-containing wing disc expressing an RNAi targeting *FasIII* mRNA. Loss of FasIII indicates RNAi efficacy and expression domain. Dotted lines indicate the positions of the indicated xz sections shown below. **(H-I')** xz sections of the wing disc shown in G showing fold morphology and FasIII. A shallowing of the M fold lacking FasIII is evident (white arrowheads). **(J-M)** xy images of wing imaginal discs stained for DNA to visualise fold morphology. *Zfh2-Gal4* expression is shown in red (J). RNAi knockdown of *Rh4* acts as a negative control whereas RNAi targeting *FasIII* or *Stat92E* disrupts the M fold (white arrows). Scale bar: in M, 100 μ m.

of clonal borders. Furthermore, localised loss of FasIII is also sufficient to remodel the three-dimensional folds normally present in the wing disc. These changes takes place in a columnar epithelial sheet with intact adherens junctions – the junctional complex that contains E-cad (Shg in *Drosophila*) and which has traditionally been thought to mediate the majority of intercellular adhesion (Adams and Nelson, 1998). Although it is not known what proportion of intercellular adhesion is being mediated by FasIII in this context, our results do suggest that the change FasIII does elicit is biologically relevant even in the context of otherwise normal adherens junctions.

Modulation of adhesion as a morphogenetic sculpting tool

Overall, our results from three diverse developmental processes – hindgut curvature, wing fold morphology and clonal boundary

straightening – show that the modulation of FasIII-mediated intercellular adhesion represents a fundamental mechanism that acts to shape three-dimensional organs during development.

In particular, the 25% reduction in local curvature of clonal boundaries separating FasIII-expressing from non-expressing regions represents both a readout for changed intercellular adhesion and a demonstration of how changes in adhesion can sculpt these clonally related cell populations. Similar clonal rounding has been previously described for other adhesion molecules, including those responsible for adherens junction integrity (Justice et al., 1995; Wei et al., 2005), and *in silico* modelling of cell sorting based on differential intercellular adhesion also demonstrates that initially random mixtures of two differentially adhesive cell populations sort out into distinct groups that seek to minimise their shared boundaries (Graner and Glazier, 1992; Graner and Sawada, 1993; Gonzalez-Rodriguez et al., 2012). Similarly, our own modelling of

the hindgut demonstrates that even comparatively modest changes in localised intercellular adhesion are able to mediate large-scale changes in organ shape and curvature. Consistent with our results, a recent report has also shown that Fasciclin II, another homophilic adhesion molecule and the *Drosophila* N-CAM (neural cell adhesion molecule) homologue, also acts to modulate membrane dynamics *in vivo* (Gomez et al., 2012).

Conservation of FasIII-like molecules?

Our work suggests that it is the changes in adhesion mediated by FasIII that are important for development and morphogenesis. Although FasIII has no direct vertebrate homologues, transmembrane adhesion molecules with similar domain structures are present in vertebrates. One example is the Ig domain-containing homophilic adhesion molecule PECAM-1 (supplementary material Fig. S6A), a protein expressed in both haematopoietic and endothelial cells (Watt et al., 1995). Strikingly, the curved tubular structure that makes up the adult mouse aortic arch also exhibits a striking asymmetry in PECAM-1 levels with significantly higher expression on the inside of the curve (supplementary material Fig. S6C,D). Although a functional role for PECAM-1 remains to be determined, the analogous increases in expression of adhesion molecules in both mouse and fly suggest that differential intercellular adhesion mediated by Ig domain-containing molecules might represent a more widely conserved characteristic of curved tissues throughout evolution. It will be intriguing to establish exactly how widespread are the roles of FasIII-like molecules in organogenesis and tissue sculpting.

Acknowledgements

We thank Barry Denholm, Nick Monk, Alex Whitworth, Stephen Brown and the Zeidler lab for valuable discussions; and Judith Lengyel, Rodger Jacob, the Bloomington *Drosophila* Stock Center and the Developmental Studies Hybridoma Bank for flies and antibodies. Imaging was undertaken at the University of Sheffield Wellcome Trust Light Microscopy Facility.

Funding

D.S. is a Wellcome Trust Senior Fellow; M.P.Z. is a Cancer Research UK Senior Cancer Research Fellow; P.E. is supported by the British Heart Foundation; R.E.W. was supported by a Biotechnology and Biological Sciences Research Council (BBSRC) doctoral training grant [BB/F017588/1]; J.D.B. and W.H. acknowledge funding from the European Commission's FP7 through the Network of Excellence 'Systems Microscopy'. Deposited in PMC for immediate release.

Competing interests statement

The authors declare no competing financial interests.

Author contributions

R.E.W., J.D.B., S.J.W. and S.C. designed and undertook experiments, analysed results and helped write the paper. P.E. and W.H. designed experiments and analysed results. D.S. and M.P.Z. designed experiments, analysed results and wrote the paper.

Supplementary material

Supplementary material available online at <http://dev.biologists.org/lookup/suppl/doi:10.1242/dev.096214/-/DC1>

References

- Adams, C. L. and Nelson, W. J. (1998). Cytomechanics of cadherin-mediated cell-cell adhesion. *Curr. Opin. Cell Biol.* **10**, 572-577.
- Arbouzova, N. I. and Zeidler, M. P. (2006). JAK/STAT signalling in *Drosophila*: insights into conserved regulatory and cellular functions. *Development* **133**, 2605-2616.
- Bach, E. A., Ekas, L. A., Ayala-Camargo, A., Flaherty, M. S., Lee, H., Perrimon, N. and Baeg, G. H. (2007). GFP reporters detect the activation of the *Drosophila* JAK/STAT pathway *in vivo*. *Gene Expr. Patterns* **7**, 323-331.
- Bellen, H. J., Levis, R. W., Liao, G., He, Y., Carlson, J. W., Tsang, G., Evans-Holm, M., Hiesinger, P. R., Schulze, K. L., Rubin, G. M. et al. (2004). The BDGP gene disruption project: single transposon insertions associated with 40% of *Drosophila* genes. *Genetics* **167**, 761-781.
- Brand, A. H. and Perrimon, N. (1993). Targeted gene expression as a means of altering cell fates and generating dominant phenotypes. *Development* **118**, 401-415.
- Brodland, G. W. (2002). The Differential Interfacial Tension Hypothesis (DITH): a comprehensive theory for the self-rearrangement of embryonic cells and tissues. *J. Biomech. Eng.* **124**, 188-197.
- Brown, S., Hu, N. and Hombría, J. C. (2001). Identification of the first invertebrate interleukin JAK/STAT receptor, the *Drosophila* gene *domeless*. *Curr. Biol.* **11**, 1700-1705.
- Campos-Ortega, J. A. and Hartenstein, V. (1985). *The Embryonic Development of Drosophila melanogaster*. Berlin; New York, NY: Springer-Verlag.
- Capdevila, J. and Guerrero, I. (1994). Targeted expression of the signaling molecule decapentaplegic induces pattern duplications and growth alterations in *Drosophila* wings. *EMBO J.* **13**, 4459-4468.
- Carthew, R. W. (2005). Adhesion proteins and the control of cell shape. *Curr. Opin. Genet. Dev.* **15**, 358-363.
- Dietzl, G., Chen, D., Schnorrer, F., Su, K. C., Barinova, Y., Fellner, M., Gasser, B., Kinsey, K., Oettel, S., Scheiblauer, S. et al. (2007). A genome-wide transgenic RNAi library for conditional gene inactivation in *Drosophila*. *Nature* **448**, 151-156.
- Gomez, J. M., Wang, Y. and Riechmann, V. (2012). Tao controls epithelial morphogenesis by promoting Fasciclin 2 endocytosis. *J. Cell Biol.* **199**, 1131-1143.
- Gonzalez-Rodriguez, D., Guevorkian, K., Douezan, S. and Brochard-Wyart, F. (2012). Soft matter models of developing tissues and tumors. *Science* **338**, 910-917.
- Graner, F. and Glazier, J. A. (1992). Simulation of biological cell sorting using a two-dimensional extended Potts model. *Phys. Rev. Lett.* **69**, 2013-2016.
- Graner, F. and Sawada, Y. (1993). Can surface adhesion drive cell-rearrangement? Part II: A Geometrical Model. *J. Theor. Biol.* **164**, 477-506.
- Gumbiner, B. M. (1996). Cell adhesion: the molecular basis of tissue architecture and morphogenesis. *Cell* **84**, 345-357.
- Hajra, L., Evans, A. I., Chen, M., Hyduk, S. J., Collins, T. and Cybulsky, M. I. (2000). The NF-kappa B signal transduction pathway in aortic endothelial cells is primed for activation in regions predisposed to atherosclerotic lesion formation. *Proc. Natl. Acad. Sci. USA* **97**, 9052-9057.
- Harrison, D. A., Binari, R., Nahreini, T. S., Gilman, M. and Perrimon, N. (1995). Activation of a *Drosophila* Janus kinase (JAK) causes hematopoietic neoplasia and developmental defects. *EMBO J.* **14**, 2857-2865.
- Hartenstein, V. (1993). *Atlas of Drosophila Development*. Plainview, NY: Cold Spring Harbor Laboratory Press.
- Hayashi, Y., Sexton, T. R., Dejima, K., Perry, D. W., Takemura, M., Kobayashi, S., Nakato, H. and Harrison, D. A. (2012). Glycans regulate JAK/STAT signaling and distribution of the Unpaired morphogen. *Development* **139**, 4162-4171.
- Hombría, J. C., Brown, S., Häder, S. and Zeidler, M. P. (2005). Characterisation of Upd2, a *Drosophila* JAK/STAT pathway ligand. *Dev. Biol.* **288**, 420-433.
- Iwaki, D. D., Johansen, K. A., Singer, J. B. and Lengyel, J. A. (2001). Drumstick, bowl, and lines are required for patterning and cell rearrangement in the *Drosophila* embryonic hindgut. *Dev. Biol.* **240**, 611-626.
- Johansen, K. A., Green, R. B., Iwaki, D. D., Hernandez, J. B. and Lengyel, J. A. (2003a). The Drm-Bowl-Lin relief-of-repression hierarchy controls fore- and hindgut patterning and morphogenesis. *Mech. Dev.* **120**, 1139-1151.
- Johansen, K. A., Iwaki, D. D. and Lengyel, J. A. (2003b). Localized JAK/STAT signaling is required for oriented cell rearrangement in a tubular epithelium. *Development* **130**, 135-145.
- Justice, R. W., Zilian, O., Woods, D. F., Noll, M. and Bryant, P. J. (1995). The *Drosophila* tumor suppressor gene *warts* encodes a homolog of human myotonic dystrophy kinase and is required for the control of cell shape and proliferation. *Genes Dev.* **9**, 534-546.
- Karsten, P., Häder, S. and Zeidler, M. P. (2002). Cloning and expression of *Drosophila* SOCS36E and its potential regulation by the JAK/STAT pathway. *Mech. Dev.* **117**, 343-346.
- Lecuit, T. and Lenne, P. F. (2007). Cell surface mechanics and the control of cell shape, tissue patterns and morphogenesis. *Nat. Rev. Mol. Cell Biol.* **8**, 633-644.
- Lehmann, R. and Tautz, D. (1994). In situ hybridization to RNA. *Methods Cell Biol.* **44**, 575-598.
- Lengyel, J. A. and Iwaki, D. D. (2002). It takes guts: the *Drosophila* hindgut as a model system for organogenesis. *Dev. Biol.* **243**, 1-19.
- Lindsley, D. L. and Zimm, G. G. (1992). *The Genome of Drosophila melanogaster*. San Diego, CA: Academic Press.
- Luo, H., Hanratty, W. P. and Dearolf, C. R. (1995). An amino acid substitution in the *Drosophila* hop^{Tum-1} Jak kinase causes leukemia-like hematopoietic defects. *EMBO J.* **14**, 1412-1420.
- Manning, M. L., Foty, R. A., Steinberg, M. S. and Schoetz, E. M. (2010). Coaction of intercellular adhesion and cortical tension specifies tissue surface tension. *Proc. Natl. Acad. Sci. USA* **107**, 12517-12522.

- Moyer, K. E. and Jacobs, J. R.** (2008). Varicose: a MAGUK required for the maturation and function of Drosophila septate junctions. *BMC Dev. Biol.* **8**, 99.
- Oshima, K. and Fehon, R. G.** (2011). Analysis of protein dynamics within the septate junction reveals a highly stable core protein complex that does not include the basolateral polarity protein Discs large. *J. Cell Sci.* **124**, 2861-2871.
- Rivas, M. L., Cobreros, L., Zeidler, M. P. and Hombría, J. C.** (2008). Plasticity of Drosophila Stat DNA binding shows an evolutionary basis for Stat transcription factor preferences. *EMBO Rep.* **9**, 1114-1120.
- Schneider, I.** (1972). Cell lines derived from late embryonic stages of Drosophila melanogaster. *J. Embryol. Exp. Morphol.* **27**, 353-365.
- Snow, P. M., Bieber, A. J. and Goodman, C. S.** (1989). Fasciclin III: a novel homophilic adhesion molecule in Drosophila. *Cell* **59**, 313-323.
- Stapleton, M., Liao, G., Brokstein, P., Hong, L., Carninci, P., Shiraki, T., Hayashizaki, Y., Champe, M., Pacleb, J., Wan, K. et al.** (2002). The Drosophila gene collection: identification of putative full-length cDNAs for 70% of D. melanogaster genes. *Genome Res.* **12**, 1294-1300.
- Tepass, U. and Hartenstein, V.** (1994). The development of cellular junctions in the Drosophila embryo. *Dev. Biol.* **161**, 563-596.
- Vidal, O. M., Stec, W., Bausek, N., Smythe, E. and Zeidler, M. P.** (2010). Negative regulation of Drosophila JAK-STAT signalling by endocytic trafficking. *J. Cell Sci.* **123**, 3457-3466.
- Watt, S. M., Gschmeissner, S. E. and Bates, P. A.** (1995). PECAM-1: its expression and function as a cell adhesion molecule on hemopoietic and endothelial cells. *Leuk. Lymphoma* **17**, 229-244.
- Wei, S. Y., Escudero, L. M., Yu, F., Chang, L. H., Chen, L. Y., Ho, Y. H., Lin, C. M., Chou, C. S., Chia, W., Modolell, J. et al.** (2005). Echinoid is a component of adherens junctions that cooperates with DE-Cadherin to mediate cell adhesion. *Dev. Cell* **8**, 493-504.
- Wright, V. M., Vogt, K. L., Smythe, E. and Zeidler, M. P.** (2011). Differential activities of the Drosophila JAK/STAT pathway ligands Upd, Upd2 and Upd3. *Cell. Signal.* **23**, 920-927.
- Zakkar, M., Chaudhury, H., Sandvik, G., Enesa, K., Luong, A., Cuhlmann, S., Mason, J. C., Krams, R., Clark, A. R., Haskard, D. O. et al.** (2008). Increased endothelial mitogen-activated protein kinase phosphatase-1 expression suppresses proinflammatory activation at sites that are resistant to atherosclerosis. *Circ. Res.* **103**, 726-732.
- Zeidler, M. P., Perrimon, N. and Strutt, D. I.** (1999). Polarity determination in the Drosophila eye: a novel role for unpaired and JAK/STAT signaling. *Genes Dev.* **13**, 1342-1353.